



## Effects of rigid bus conductors on seismic fragility of electrical substation equipment



Amir Gh Baghmisheh\*, Homayoon E. Estekanchi

Department of Civil Engineering, Sharif University of Technology, Tehran, Iran

### ARTICLE INFO

#### Keywords:

Fragility curves  
Interconnected substation equipment  
Dynamic interaction  
Circuit breaker  
Disconnect switch  
Current transformer  
Surge arrester

### ABSTRACT

The present paper studies the impact of dynamic interaction between high-voltage substation equipment on the response and vulnerability of substation equipment. The 3D numerical model is developed for four types of vulnerable equipment in the both unconnected and connected conditions. The bus slider-rigid bus assembly is utilized to establish the connection between the equipment. The incremental dynamic analysis is carried out in the developed systems to produce the fragility function for each equipment. Also, the Monte Carlo approach is employed to evaluate the accuracy of the generated functions. It is concluded that the incorporation of connection parts in the model can significantly alter the fragility of equipment and the relative performance of vulnerable equipment. Moreover, it is found that when more than two equipment are connected, the effect of indirectly connected equipment can be neglected if the contribution of higher modes to its response is small. The fragility functions for which the interaction effects are accounted can be used to reliably assess the seismic risk of substations.

### 1. Introduction

Electrical substations are the nodes of power transmission network which their continuous operation after earthquakes has paramount importance for the well-being of community. The damage of earthquake to substations may impose disruption in rescue operation after the earthquake and in the performance of other critical lifelines such as water delivery systems.

Substations are composed of various types of equipment such as surge arrester (SA), current transformer (CT), circuit breaker (CB), disconnect switch (DS), etc., which are connected through the conductors. Most equipment include slender ceramic insulators under a large concentrated mass, which increases the vulnerability to the earthquake-induced forces [1–3]. Moreover, conductors result in the interaction between the equipment with different dynamic characteristic, which in turn can contribute to their vulnerability [4]. Also, as the voltage level of substation is increased, the fragility of its component is increased accordingly.

The interconnection between the equipment are provided through the rigid bus assemblies or flexible cables as conductor. Rigid buses include an aluminum pipe with a flexible connector at one end. Two types of common connectors are the flexible strap connector (FSC) and bus slider (BS). Although connectors are originally designed for the thermal expansion purposes, they increase the flexibility and

dissipation capacity of conductors, which may lead to the reduction in the adverse interaction effects. However, the transfer of force between equipment, variations of dynamic properties and exceedance of connectors' displacement limit may cause severe interaction effects. Depending on the slack, cables may increase or decrease the response of equipment. Thus, the interconnected equipment has become a complex dynamic system.

Seismic qualification of equipment is usually performed without considering the interaction effects ([1,2,5–7]). This is due to the diversity of connected equipment and conductors in substations. Also, it is not usually practical to conduct the shaking table test on several interconnected equipment due to the budget and laboratory restrictions. Although some new methods, such as real-time hybrid simulation (RTHS) developed by Mosalam and Gunay [8], are presented to conduct tests on the interconnected equipment, they need intelligent facilities which are not simply available. Therefore, the accurate numerical methods can be employed to evaluate the effects of connection between equipment on the response and vulnerability.

In late 1990s, PEER began a project in collaboration with PG&E to examine the interaction effects between equipment in substations and to introduce guidelines for mitigating these effects. In the first step, Der Kiuregian et al. [4] numerically investigated the interaction between two equipment. They modeled the equipment as SDOF systems and the rigid bus assembly as linear spring-dashpot-mass. An extensive

\* Corresponding author.

E-mail address: [Amirghb73@gmail.com](mailto:Amirghb73@gmail.com) (A.G. Baghmisheh).

parametric study was done to evaluate the effect of different system parameters on the interaction. Then, an experimental study was conducted at UCSD to produce validation data for the numerical analysis [9]. They performed cyclic tests on three types of FSC and one type of BS connectors. Also, they carried out shaking table test on five pairs of simulated equipment connected through the rigid bus assemblies. Following the PEER project, Der Kiuregian et al. [10] extended previous linear connector to a nonlinear one using the detailed FEM. They also developed a mathematical model for the FSC-rigid bus assembly by fitting hysteresis cycles to the ones obtained in Ref. [9]. The effect of flexibility and energy dissipation of FSCs on the interaction results is investigated through the parametric study. It should be noted that only two recorded ground motions were used in this study. In 2004, a quasi-static cyclic test was conducted on two improved connectors in Ref. [11]. They investigated the interaction effect for the equipment connected by these modified connectors through the shaking table test. Afterwards, Song et al. [12] developed a mathematical model for all rigid bus connectors tested in Refs. [9,11]. Finally, Dastous and Der Kiuregian [13] proposed a design procedure where the interaction effects are taken into account with simple relations. In addition to PEER project, different methodologies have been developed for the seismic design of conductors considering the interaction effect [14,15].

The assessment of interaction in the PEER project has some limitations: (a) The higher-mode effects on the responses are not taken into account, because SDOF systems are incorporated for modeling the equipment, (b) Only the pairs of interconnected equipment are studied and the influence of more than two connected equipment is not investigated, and (c) A limited number of records are used and only one component is incorporated in the analysis. In Ref. [16], limitation of two-connected systems were addressed for the cable-connected equipment.

The evaluation of vulnerability in various substation equipment was conducted both in an experimental and numerical manner. In 1999, Anagnos [17] developed a database according to the damaged and undamaged equipment for the twelve previous earthquakes in California which is used to construct the experimental fragility curves. Since the data collected for each individual equipment was limited, the rough estimation of vulnerability was presented. In addition, HAZUS [18] proposed the fragility parameters for the equipment based on the failure observed in some substations. Paolacci et al. [3] derived analytical fragility functions for high-voltage DS. They investigated the sensitivity of functions to DS dynamic parameter and concluded that the characteristics of bottom joints have the most substantial effect on the fragility. Zareii et al. [19] evaluated the vulnerability of CB using the multivariate fragility functions. The vulnerability assessment of other equipment like power transformer was also reported in literature [20,21]. In all previous numerical studies, the fragility functions have been developed for the stand-alone configurations without considering the effect of conductors and adjacent equipment.

Regarding the gap existing in the literature, this study aims to: (1) evaluate the effects of record-to-record and intensity variations on the interaction results when more than two equipment are connected to each other, (2) generate vulnerability functions of interconnected equipment and compare them with the stand-alone ones, and (3) investigate how many connected equipment may have considerable effects on the fragility.

In the present study, the 3D numerical model of 400 kV equipment including SA, CT, CB and DS was developed and verified in their stand-alone configuration. A mathematical model was incorporated to model the hysteretic behavior of BS employed to connect four equipment to each other. Also, the nonlinear time history responses of BS-rigid bus assembly were validated. Then, the incremental dynamic analysis (IDA) with three-component records was carried out on the both unconnected and connected models. The variations of equipment responses due to

the conductors were measured by dividing the connected system responses to the unconnected ones. The IDA results were also used to estimate the parameters of fragility functions for each equipment in the stand-alone and interconnected conditions. This procedure was repeated for each equipment in which different interconnected systems were considered. Meanwhile, the Monte Carlo sampling approach was employed to investigate the accuracy of developed fragility curves. Finally, in order to have an overall view on the interaction effects, the hazard curve of a site in Tehran and the fragility curves of equipment were convolved to produce the mean annual rate of failure.

## 2. Method

### 2.1. Incremental dynamic analysis

IDA is a structural analysis procedure which is employed to collect data for developing the fragility [22]. To perform IDA, several ground motion records are scaled progressively for various intensity levels and applied to numerical model. In the present study, peak ground acceleration (PGA) is chosen as the intensity measure (IM) to scale the records. One horizontal component of each record is increased in amplitude by an increment of 0.1 g up to 1.5 g, while other components are scaled so that the as-recorded ratio of peak acceleration among components remains constant. After the completion of IDA, the responses resulted from each ground motion set is traced versus the intensity measure to obtain the PGA values at which the demand exceeds capacity. These are required data for the fragility generation.

### 2.2. Fragility generation

Fragility functions show the probability of exceedance of a certain damage level given an intensity measure and are usually described as lognormal cumulative distribution function:

$$P \left[ \text{Damage} \geq DS_i | IM = x \right] = \Phi \left( \frac{\ln(x/\theta)}{\beta} \right) \quad (1)$$

Where  $P[\text{Damage} \geq DS_i | IM = x]$  is the probability that damage exceeds  $DS_i$  threshold when  $IM$  is equal to  $x$ ,  $\Phi()$  denotes the standard normal cumulative distribution function,  $\theta$  is equal to the intensity measure with 50% probability of exceedance (median), and  $\beta$  denotes the standard deviation of  $\ln IM$ . The estimation of fragility parameters (i.e.,  $\theta$ ,  $\beta$ ) is a statistical procedure and depends on the method used to perform structural analysis [23]. In this study, since the IDA approach was used for collecting data to find the fragility parameters, the moment method described below was chosen to estimate the parameters [24].

As mentioned in section 2.1, the incremental dynamic analysis results in  $IM$  values for each ground motion set where the structure response exceeds the limit state of interest. Taking natural logarithm of these  $IM$  values and calculating the mean and standard deviation lead to the estimation of fragility parameters as follows [23,24].

$$\ln \hat{\theta} = \frac{1}{n} \sum_{i=1}^n \ln IM_i \quad (2)$$

$$\hat{\beta} = \sqrt{\frac{1}{n-1} \sum_{i=1}^n (\ln(IM_i/\hat{\theta}))^2} \quad (3)$$

Where  $n$  is the total number of ground motion in the set and  $IM_i$  is the  $IM$  value in which the exceedance of damage threshold for the  $i$ th ground motion occurs. It should be noted that the moment method is applicable when the responses of all ground motions reach the damage threshold at the intensity values smaller than the maximum ones considered in IDA. If some ground motion in the set does not reach the

threshold, other parameter estimation methods like maximum likelihood may be employed [23].

The PGA is the intensity measure used to represent fragility curves. This selection is based on several reasons. First, PGA is a commonly used intensity measure for the vulnerability evaluation of electrical equipment ([18–20]). It provides an opportunity to compare fragility results obtained here with the previous ones. Second, it makes it easy to employ IEEE693 [25] design spectra. This is because, in contrast with building design code ASCE7 [26] where the design spectrum is described by spectral ordinate at two period, the IEEE standard's spectrum is based on spectral ordinate at zero period (i.e., PGA). Finally, since fragility functions only depend on PGA, they can be incorporated in the seismic risk analysis of any location without the need to involve information on dynamic characteristic of equipment (For example, natural frequency).

The states of significant damage to substation equipment can be classified as: cracking of insulator, leakage of oil, fracture of insulator, disconnection of conductor, and failure of supporting structure. Among these states, the latter has been rare in previous earthquakes [19]. Two damage states are considered for the vulnerability evaluation of equipment similar to Refs. [19,27]. The moderate damage state is supposed to be associated with the development of fine cracks at the outer surface of insulator, which may change the insulation properties. The major cracking is assumed as severe damage state, which may cause the oil leakage from the insulator and in turn lead to loss of functionality of equipment. Because high uncertainty involved in determining fracture point of equipment, this damage state is not considered. Furthermore, since this study aims to compare the vulnerability of equipment in the stand-alone and connected systems, the disconnection of conductor is not considered as damage state for the connected systems. However, it will be demonstrated that severe damage state occurred before the disconnection of conductor for all studied cases.

Determining the damage state threshold is based on IEEE recommendation. Version 1984 and 2005 of this standard suggest 25% and 50% of porcelain ultimate stress as the allowable stress [25]. In the present study, 25% of ultimate stress is selected as the moderate threshold and 50% of ultimate stress is chosen as the severe threshold. Because overcoming half of the porcelain strength are not allowed by IEEE provisions for the design of equipment, the latter damage state is considered corresponding to this threshold. Although it can be interesting to consider damage state corresponding to the overcoming of total ceramic strength, this is not considered because of the restrictions of numerical models, which will be explained in section 3.6. The ultimate strength of porcelain is assumed to be 50.511 MPa. The damage thresholds described here are consistent with those presented in previous fragility studies on the equipment ([19,21,27]).

As mentioned, two damage states are considered here, and the collapse fragility is not incorporated in the study. This is because of high uncertainty involved in the determining fracture point of equipment. As depicted in experimental studies like ([6,28]), collapse usually occurs at stress levels which are almost 20 to 30 percent higher than the strength specified by manufacturer. Difference between actual strength and manufacturer proclamation is attributed to that companies consider a safety factor which usually is not reported. On the other hand, premature collapse may occurs depend on property of major cracks. Therefore, more detailed finite element model or experimental test is required to accurately capture collapse point, which can be subject of future studies.

It should be noted that despite building structure where the collapse prevention is crucial for saving people's lives, the main objective of electrical structures is to remain functional after a severe earthquake. Furthermore, in the both case of loss of functionality and completely collapse of equipment, the retrofit strategy is usually a replacement for

the equipment. Thus, in the case of substation equipment, the utility managers are more interested in reducing the risk of loss of functionality.

### 2.3. Statistical efficiency of fragility estimations

In order to assess the efficiency of IDA in estimating the fragility parameters, the Monte Carlo approach is employed which is generally proposed by Baker [23]. In this approach, it is assumed that the considered fragility parameters are a true one, and then, the accuracy of this assumption is investigated through simulating the synthetic structural analysis data. The procedure can be summarized in four steps as follows:

- 1) Assume the fragility function parameters as true one and produce a lognormal random variable for the intensity measure based on the parameters.
- 2) Generate the realization for the random variable (i.e., IM values that cause failure) as many as the number of considered ground motions in IDA.
- 3) Estimate fragility parameter using Equations (2) and (3) based on produced data from step 2.
- 4) Repeat step 2 and 3, N times ( $N > 1$ ) to evaluate the variability of estimated parameters in comparison with the original ones (i.e., parameters of step 1).

### 2.4. Failure probability

In order to calculate the mean annual rate of failure, the seismic hazard curve for a site should be integrated over the fragility curves as the following equation ([24,29,30]):

$$\lambda_{\text{failure}} = \int_x P[\text{failure} | IM = x] \cdot d\lambda_{IM}(x) = \int_x \Phi\left(\frac{\ln(x/\theta)}{\beta}\right) \cdot \left| \frac{d\lambda_{IM}(x)}{d(x)} \right| d(x) \quad (4)$$

where  $\lambda_{\text{failure}}$  is the mean annual frequency of failure and  $\lambda_{IM}$  is the mean annual rate of exceedance of the intensity measure. Calculating above equation requires the numerical solution in which the integral is discretized into the summation. In this process, the absolute slope of hazard curve at each small IM step is multiplied by the corresponding failure probability in the fragility curve and multiplied by the size of step and then, the obtained results are added over all IM steps [30].

If the occurrence of earthquakes follows a Poisson distribution over time, the mean annual rate of failure can be transformed to the probability of failure in  $t$  years as follows:

$$P_{\text{failure}}(\text{in } t \text{ years}) = 1 - \exp(-\lambda_{\text{failure}} \cdot t) \quad (5)$$

## 3. Numerical modeling of equipment and conductors

### 3.1. General specifications of equipment

The equipment considered in this study are shown in Fig. 1, which are generally composed of hollow ceramic insulator columns connected together through steel flange joints. According to previous experimental study ([6,31]), the coupled system of insulator columns and flange joints have linear behavior until a sudden collapse. However, the deformability of joints may contribute to the slightly hysteretic behavior, which is observed in some cyclic tests such as those in Ref. [1]. Therefore, the porcelain columns and flange joints demonstrate various stiffness and flexibility. In addition, the jagged insulators and cemented joints introduce complexity in determining the structural properties. Hence, the experimental studies or regression models calibrated

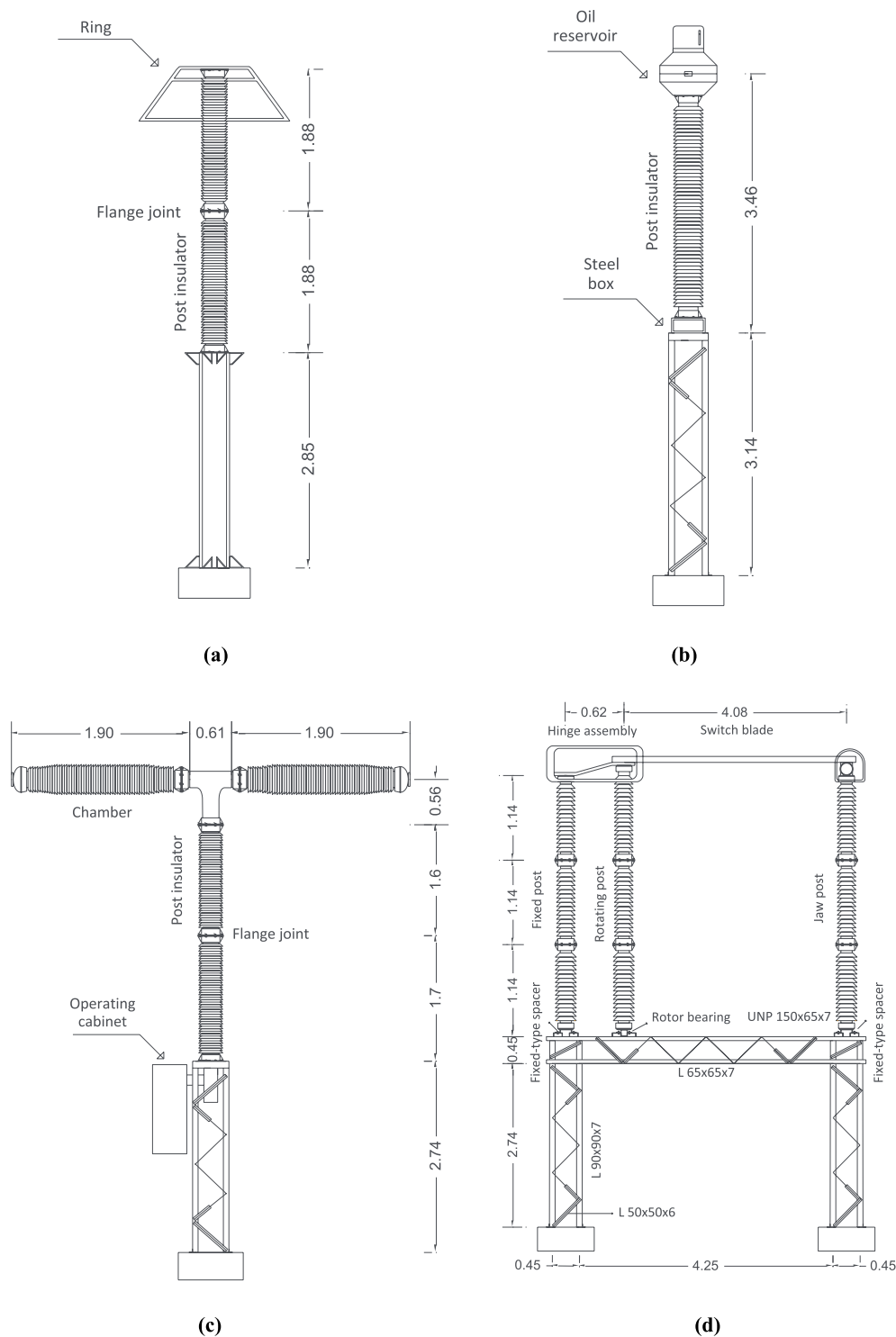


Fig. 1. Schematic drawings of equipment (a) surge arrester (b) current transformer (c) circuit breaker (d) disconnect switch.

through the test are used to determine equivalent bending stiffness of insulators and rotational stiffness of joints.

The numerical model is implemented in OpenSees software [32]. The linear beam-column elements with equivalent pipe section and linear rotational springs are adopted for modeling the insulators and joints, respectively. The nonlinear DispBeamColumn elements with fiber sections are used to model the steel supports. The self-weight of insulators and steel elements are considered as uniformly distributed mass. Also, the additional masses at top of equipment or supporting structures are treated as the concentrated mass. The fixed-type support

is assumed as the boundary condition of steel structure and the soil-structure interaction is neglected. Fig. 2 shows the numerical model of considered equipment.

The equipment in the stand-alone configuration have linear behavior, because the linear material is used for constructing models. Although the nonlinear elements are utilized to model the supporting structures, the nonlinear behavior in those elements is not observed in none of the analyzed cases. It should be noted that due to the low level of ductility, the equipment usually has brittle failure, and its behavior after failure is not considered in the models.

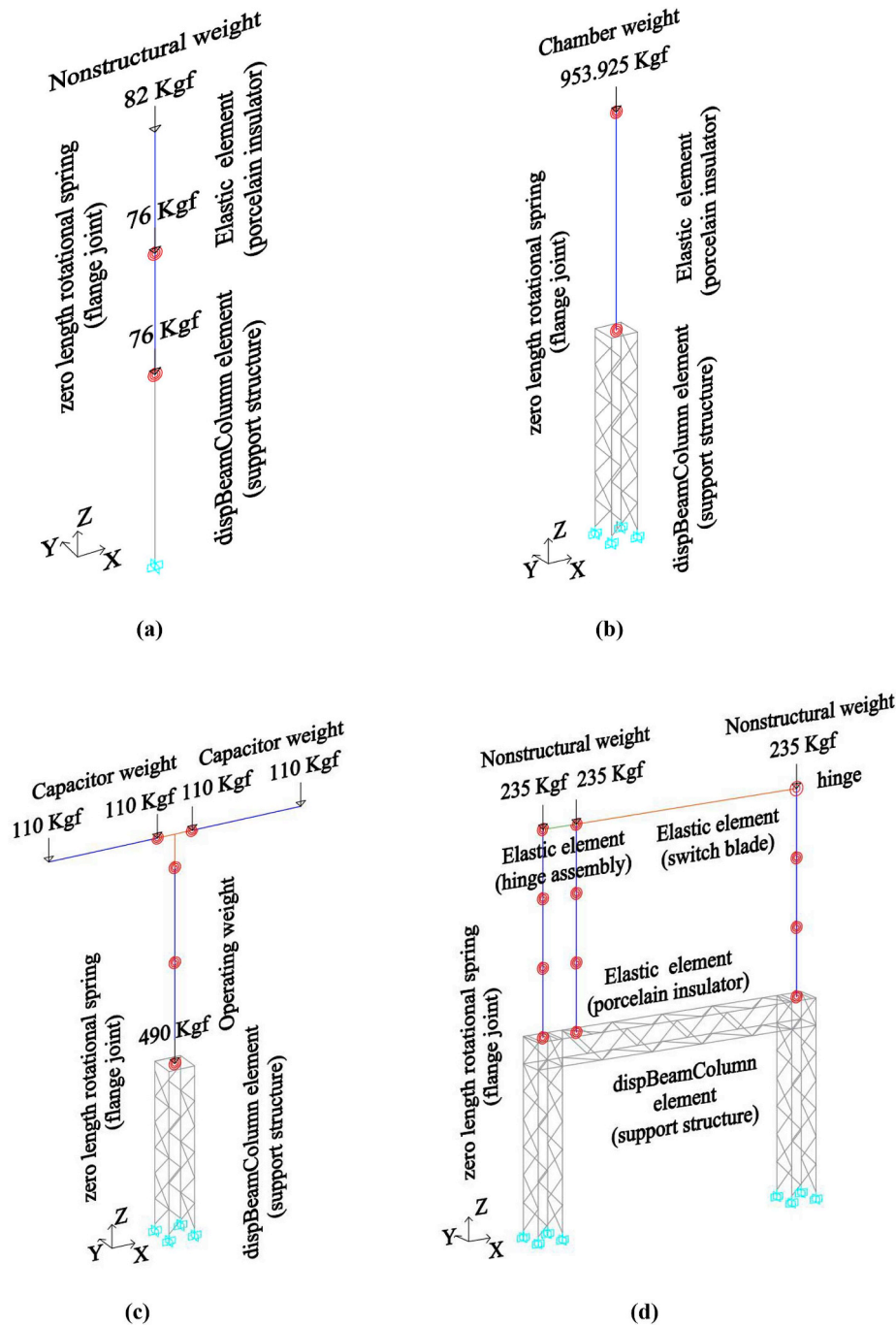


Fig. 2. Numerical model of (a) surge arrester (b) current transformer (c) circuit breaker (d) disconnect switch.

The procedure of verification is different for the equipment in the stand-alone and interconnected configuration. Because behavior of stand-alone equipment is linear, the natural frequency evaluation test or information provided by manufacturer on the natural frequency are used for the verification. Moreover, due to the diversity of supporting structures used in the substations, the seismic qualification tests on the equipment are usually conducted without the supporting structure. Thus, the verification of numerical model is carried out on equipment configuration without the structures on which they are mounted. On the other hand, Due to the nonlinearity introduced by BS in the interconnected system, the existing shaking table tests in the literature on a pair of steel beams connected by BS-rigid bus assembly are utilized to assess the response accuracy of components connected by BS.

Because the components of individual equipment, method of

determining structural parameters, and evaluation of accuracy are different from one another, separate sections are allocated for each equipment as follows.

### 3.2. Surge arrester

As seen in Fig. 1a, high-voltage surge arresters include two or three insulator columns and several grading aluminum rings on top. The assembly is usually installed on a varying-height supporting structure to satisfy electrical requirements [2].

The surge arrester considered in this study is almost the same as the one tested in Ref. [2] with two exceptions to adjust with nearby equipment. First, two porcelain insulators are used instead of three. Second, the height of supporting structure is assumed as 2.85 m instead

of 4 m. Therefore, the numerical model of SA in Ref. [2] is developed and verified through the frequency evaluation test. Then, the required changes are made on the model to be appropriate for the present study.

In order to determine the flexural rigidity of insulators and rotational stiffness of joints, the regression models proposed in Ref. [33] are employed here. The models were developed based on the data collected from the twelve experimental tests on the large dimension insulators along with the flange joints. Furthermore, they are verified through the shaking table test on the surge arresters in Ref. [2]. These relations are summarized below [33].

The flexural rigidity of jagged porcelain column can be estimated:

$$EI_s = \lambda_s EI_{eq} \quad (6)$$

where

$$\lambda_s = 1.045 + 5 \times 10^{-3} D_c^{-2} \quad (7)$$

and  $0.215m < D_c < 0.7m$ .

$$EI_{eq} = (1/64)\pi(D_c^4 - d^4)E_p \quad (8)$$

The rotation stiffness of the flange can be calculated as follows:

$$K_c = \lambda_c D_c h_c / t_c \quad (9)$$

where

$$\lambda_c = 5.25 \times 10^7 h_c \text{ where } 0.075m < h_c < 0.35m \quad (10)$$

$$\lambda_c = 6.54 \times 10^7 h_c \text{ where } h_c < 0.075m \quad (11)$$

Where  $D_c$  and  $d$  are the outer and inner diameter of jagged insulator, respectively.  $E_p$  is the elasticity modulus of porcelain.  $h_c$  and  $t_c$ , respectively, are the height and thickness of cement attaching the flange joint and porcelain together. The structural parameters of SA and its supporting structure are listed in Table 1 and Table 2, respectively. The modal analysis was carried out on the equipment and the resulting frequencies for the first five modes are reported in Table 3.

### 3.3. Current transformer

Current transformer is an assembly of a large dimension hollow insulator, an oil reservoir at tip of ceramic column and a steel box at bottom of the lowest flange joint where the equipment is connected to the supporting structure. Fig. 1b schematically illustrates this equipment. For this particular equipment, in contrast with previous one, the existence of steel box in addition to flange joint introduces further flexibility that should be considered in the modeling. Thus, a linear rotational spring in series with flange joint spring was adopted to reproduce the behavior of connection between CT and its support. The stiffness of flange joint and insulator is calculated through Equations (6)–(11). In order to estimate the stiffness of the spring representing the steel box, the modal analyses are performed on CT assembly without the supporting structure, and the spring stiffness is adjusted so that the natural frequency of analysis to be identical with the one declared by the provider (3.80 Hz without steel support). The total stiffness

**Table 1**  
Structural parameters of surge arrester.

Position of porcelain unit	Top	Bottom
Weight (N)	2530.98	2530.98
Height (m)	1.88	1.88
Concentrated mass at top (kg)	82.6	44
Concentrated mass at bottom (kg)	32	76.5
Young 's modulus of porcelain, $E_p$ (Pa)	$9 \times 10^{10}$	$9 \times 10^{10}$
Inner diameter, $d$ (m)	0.353	0.353
Outer diameter, $D_c$ (m)	0.37	0.37
height of cement, $h_c$ (m)	0.09	0.09
Thickness of cement, $t_c$ (m)	$7.5 \times 10^{-3}$	$7.5 \times 10^{-3}$
flange joint stiffness, $K_c$ (N m/rad)	$13.55 \times 10^6$	$13.55 \times 10^6$

calculated for the series spring along with other structural specifications of CT are listed in Table 4. It should be noted that the mass of oil inside the ceramic column along with the mass of ceramic column are considered as the uniformly distributed mass, and the amount of oil accumulated at top reservoir is treated as the lumped mass.

The lattice steel structure is used as the support for the CT. This structure is composed of four columns joined together at top through four beams. Also, the diagonal braces along the length of columns provide lateral stiffness for the structure. In addition, a steel plate is located on beams and connected with bolts. Due to the relatively high thickness of plate, it is treated as rigid diaphragm in the numerical model. The geometric configuration of structure and section of elements are presented in Fig. 2 and Table 2, respectively.

### 3.4. Circuit breaker

As shown in Fig. 1c, the considered CB is consisted of a ceramic column with two vertically connected insulators and two horizontal chambers which are connected to column through flange joint. Two horizontal capacitors are also attached to each side of chambers. Similar to CT, CB rests on a lattice structure, and a cabinet as the house of electrical component is laterally linked to top of the supporting structure.

The regression relations (Equations (6)–(11)) are employed here to estimate the structural parameters. Capacitors and cabinet are assumed as nonstructural component and modeled as lumped mass. The structural characteristic of CB and supporting structure are listed in Table 5 and Table 2, respectively.

The study CB has similar configuration to one investigated in Ref. [34] with several differences in geometry of equipment and supporting structure. Hence, the frequency results of this study are compared with those evaluated here. As reported in Table 3, the natural frequency of CB is 2.02 Hz, which is almost consistent with 2.38 Hz achieved in Ref. [34]. This slight difference can be attributed to the little difference in the configuration.

### 3.5. Disconnect switch

The study high-voltage DS is composed of three posts entitled as fixed, jaw and rotating posts based on the electrical performance. Each post includes three ceramic columns. Fixed and jaw posts are installed on steel spacers, while rotating post is mounted on rotor bearing, as shown in Fig. 1d. An hinge assembly connects fixed posts to the rotating ones which in turn are connected to jaw post through switch blade ([7,35]). The entire assembly of DS is mounted on a supporting frame.

As mentioned before, the connection of each post to supporting structure is different from one another because of electrical requirements, and is also different from middle flange joint. To determine the bending stiffness of these connections, the experimental frequency evaluation test is required which has been conducted on each post at separate tests. On the other hand, to the best of the authors' knowledge, there is no experimental study that can satisfy these criteria for the 400 kV disconnect switch. Therefore, the test conducted in Ref. [7] on the 230 kV disconnect switch is utilized here, which has almost identical dimension to two upper insulators of each 400 kV post. After constructing a numerical model for each test, the frequency evaluation is performed and the connection stiffness is adjusted to reproduce the natural frequency identical to the test. Although the bottom units of 400 kV posts have slightly larger dimension than the ones of 230 kV posts, it is assumed that the stiffness adjusted for the spacers and rotor bearing is applicable to 400 kV DS. It should be noted that due to the smaller dimension of two upper insulators of each post than the minimum allowable range of regression relations (Equations (6)–(11)), the test on the assembly of ceramic insulator and flange joint in Refs. [3,7] is also utilized here to determine the stiffness of middle flange joints and the rigidity of insulators. The structural parameters needed

**Table 2**  
Key parameters of supporting structure for each equipment.

Item	Column section	Beam section	Brace section	Height	Young's modulus
Surge arrester	C400 × 10	–	–	2.85 m	2 × 10 <sup>5</sup> MPa
Current transformer	L80 × 80 × 8	L100 × 100 × 10	L50 × 50 × 5	3.14 m	2 × 10 <sup>5</sup> MPa
Circuit breaker	L80 × 80 × 8	L100 × 100 × 10	L50 × 50 × 5	2.74 m	2 × 10 <sup>5</sup> MPa
Disconnect switch	L90 × 90 × 7	L65 × 65 × 7	L50 × 50 × 6	3.18 m	2 × 10 <sup>5</sup> MPa

**Table 3**  
Modal frequency of equipment.

Item	Mode 1	Mode 2	Mode 3	Mode 4	Mode 5
Surge arrester	4.45	4.45	19.85	19.85	43.2
Current transformer	3.64	3.64	22.38	22.58	106.68
Circuit breaker	2.02	2.32	3.54	6.58	14.63
Disconnect switch	1.44	1.45	2.65	18.33	18.94
Four-connected equipment system	1.77	2.62	2.96	3.33	3.93

**Table 4**  
Structural parameters of current transformer.

Direction of porcelain unit	vertical
Weight (N)	8103.75
Height (m)	3.46
Concentrated mass at top (kg)	953.92
Young's modulus of porcelain, E <sub>p</sub> (Pa)	10 × 10 <sup>10</sup>
Inner diameter, d (m)	0.442
Outer diameter, D <sub>c</sub> (m)	0.48
height of cement, h <sub>c</sub> (m)	0.12
Thickness of cement, t <sub>c</sub> (m)	12.5 × 10 <sup>-3</sup>
flange joint stiffness at top (bottom), K <sub>c</sub> (N m/rad)	24.19 (11.04) × 10 <sup>6</sup>

for modeling the DS are presented in Table 6.

The modeling procedure is the same as previously described equipment with some differences. Each individual post, in addition to the spacers, is bolted to two channel sections (UNP 150 × 65 × 7) and then mounted on the frame. Due to the influence of these elements on flexibility, they are modeled as linear beam-column elements. Moreover, the switch blade and hinge assembly with circular 100 × 5 steel pipe and 100 × 100 × 6 steel box sections, respectively, are also presented through the beam-column elements. In case of switch blade, at the end connected to rotating post, the moment is released for the in-plane rotation of DS, while the moment is released for both in-plane and out-of-plane rotations at the other end. In the hinge assembly, the both ends are considered moment-released only for the in-plane rotation [7]. The support frame, as shown in Fig. 2d, is composed of angle sections

**Table 5**  
Structural parameters of circuit breaker.

Position of porcelain unit	Vertical		Horizontal	
	Top	Bottom	Left	Right
Weight (N)	1384.78	1552.82	3757.72	3757.72
Height (m)	1.6	1.7	–	–
Length (m)	–	–	1.9	1.9
Concentrated mass at top (kg)	5	5	–	–
Concentrated mass at bottom (kg)	5	490	–	–
Concentrated mass at left (kg)	–	–	110	110
Concentrated mass at right (kg)	–	–	110	110
Young's modulus of porcelain, E <sub>p</sub> (Pa)	10 × 10 <sup>10</sup>	10 × 10 <sup>10</sup>	10 × 10 <sup>10</sup>	10 × 10 <sup>10</sup>
Inner diameter, d (m)	0.328	0.333	0.401	0.401
Outer diameter, D <sub>c</sub> (m)	0.342	0.348	0.441	0.441
height of cement, h <sub>c</sub> (m)	0.12	0.12	0.09	0.09
Thickness of cement, t <sub>c</sub> (m)	12.5 × 10 <sup>-3</sup>	12.5 × 10 <sup>-3</sup>	12.5 × 10 <sup>-3</sup>	12.5 × 10 <sup>-3</sup>
flange joint stiffness at top (bottom), K <sub>c</sub> (N m/rad)	5.51 (10.93) × 10 <sup>6</sup>	10.93 (13.61) × 10 <sup>6</sup>	10.55 × 10 <sup>6</sup>	10.55 × 10 <sup>6</sup>

**Table 6**  
Structural parameters of disconnect switch.

Position of porcelain unit	Top	Middle	Bottom
Weight (N) <sup>a</sup>	575.45	770.08	1062.23
Height (m)	1.14	1.14	1.14
Concentrated mass at top (kg) <sup>a</sup>	235	10	10
Young's modulus of porcelain (Pa)	10 × 10 <sup>10</sup>	10 × 10 <sup>10</sup>	10 × 10 <sup>10</sup>
Inner diameter (m)	0.117	0.13	0.146
Outer diameter (m)	0.172	0.197	0.23
joint stiffness of fix post (N m/rad)	1.85 × 10 <sup>6</sup>	1.85 × 10 <sup>6</sup>	0.39 × 10 <sup>6</sup>
joint stiffness of rotating post (N m/rad)	1.85 × 10 <sup>6</sup>	1.85 × 10 <sup>6</sup>	0.31 × 10 <sup>6</sup>
joint stiffness of jaw post (N m/rad)	1.85 × 10 <sup>6</sup>	1.85 × 10 <sup>6</sup>	0.39 × 10 <sup>6</sup>

<sup>a</sup> Values for one post are reported here.

which are listed in Table 2. The modal analysis results of this equipment as other ones are summarized in Table 3.

### 3.6. Rigid bus conductor

Despite the linear and brittle behavior of equipment, the intermediate conductor is usually composed of ductile connector which can dissipate energy during the seismic excitation. The BS-rigid bus assembly used to connect equipment to each other consists of an aluminum pipe and a bus slider at one end. As seen in Fig. 3a, the bus slider includes two pairs of looped cable which is welded on the pipe from one side and attached to terminal pad from other side, a bulged-end shaft that slides into pipe, and a terminal pad connecting equipment to conductor. The cables produce the elastic-resisting force and the shaft generates the friction force in contact with the inner surface of pipe when the equipment moves relative to each other. Thus, a combination of elastic and Coulomb-type friction behavior occurs, which produce flexibility and dissipation capability for the conductor [9]. When the slider displacement limit exceeds in compression, the contact occurs between the pipe and the equipment, and when exceeds in tension, the shaft slides out from the pipe. The stroke capacity of bus slider in both tension and compression is measured as 8.89 cm in cyclic test in Ref. [9]. In this study, the improved bus sliders with larger stroke capability containing the stopper are not utilized for preventing the

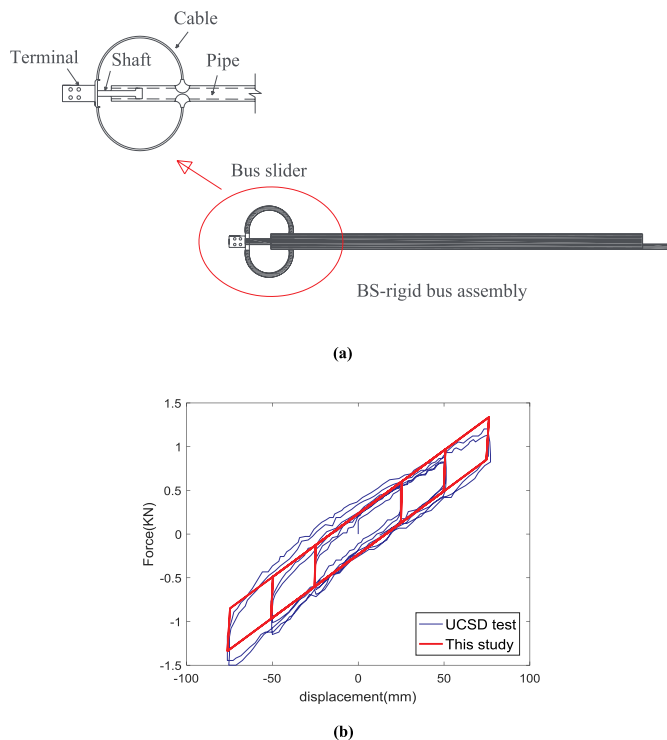


Fig. 3. (a) Schematic of BS-rigid bus assembly and bus slider (b) comparison between hysteretic cycles of experiment in Ref. [9] and those of numerical model in this study.

pullout of shaft.

The results of quasi-static cyclic test on the bus slider conducted in Ref. [9] at UCSD is served to construct a numerical model. The

specimen was tested under the given displacement history in the axial direction of pipe. Displacement transducer and load cells of test machine were used to obtain the force-displacement hysteresis loops. The movement of shaft outward and inward the pipe is considered as the negative and positive displacement, respectively. As can be seen in Fig. 3b, the bilinear hysteresis curves are observed during the test. The preliminary force and displacement for the slide to begin is estimated as 240 N and 0.0203 cm, respectively. The post slip stiffness induced by elastic flexural deformation of cables is measured as 15 N/mm [9]. According to these parameters, Steel01 was used in an axial spring to reproduce this nonlinear behavior. The reason for choosing this simple model is that it is very complicated to construct a finite element model representing the coupled behavior of elastic and coulomb friction. The dependence of friction force on the shaft alignment causes this complexity, which is usually impractical to measure in the field conditions [12]. Another idealization is that the behavior of BS beyond its stroke limit is not considered in the numerical model. The absence of a test going beyond the displacement limit or a detailed finite element model accounting for the impact between BS-rigid bus assembly and equipment for verifying the numerical model was the reason for this simplification assumption. The influence of this assumption on the fragility results is discussed in section 5.2.

The hysteretic cycles of BS numerical model are compared with the experimental results in Fig. 3b. As can be seen, a satisfactory level of accuracy was achieved. Note that this model accounts for all material and geometric nonlinearities involved in BS, because its hysteretic cycles are adopted based on the experimental tests.

### 3.7. Validation of nonlinear time history response

In this section, the nonlinear time history response of BS-rigid bus assembly is validated. To the best of the authors' knowledge, there is no shaking table test on real device interconnected by BS. The test carried out on two vertical steel beams interconnected by BS-rigid bus assembly

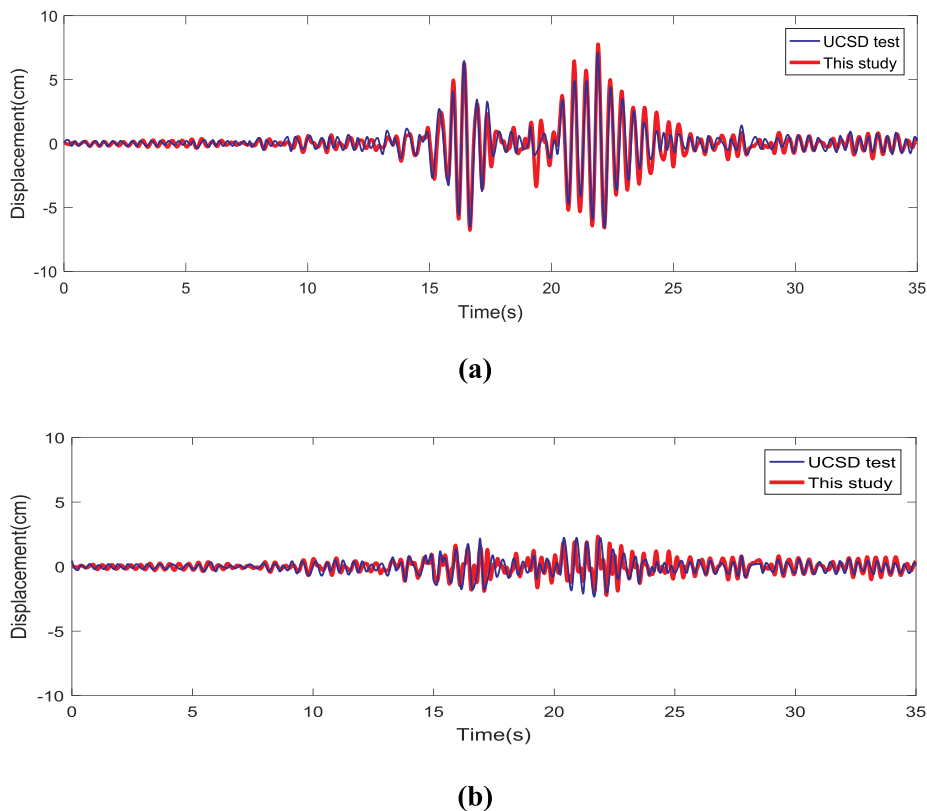


Fig. 4. Comparison between displacement time history of test in Ref. [11] and present study for (a) soft and (b) stiff beam in connected system.

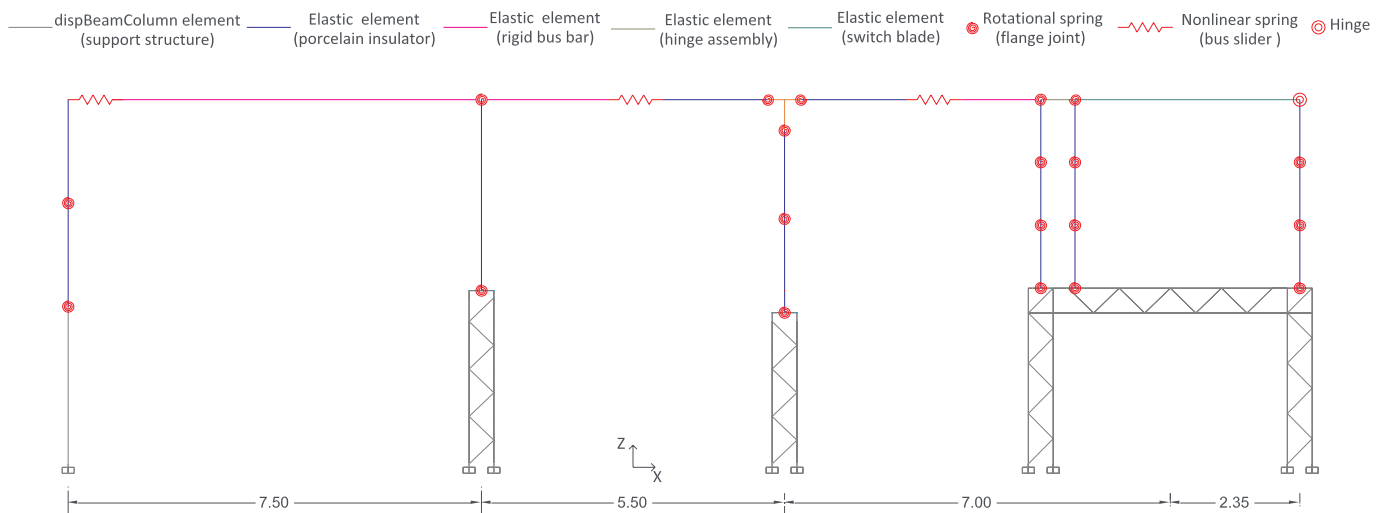


Fig. 5. Numerical model of interconnected system of equipment.

is served here for the accuracy evaluation. In order to develop the numerical model of test, a simple linear BeamColumn element is utilized to represent the beams and bilinear spring adjusted to model the BS. Then, according to test sequence called RB-79 [11], the modified version of Tabas (1979, Iran) ground motion recorded on the shaking table is imposed on the model in the axial direction of bus bar. The comparison between displacement time histories at top of each beam in numerical analysis and the corresponding ones in experimental test is illustrated in Fig. 4. A relatively high level of matching between the responses indicates the adequacy and accuracy of considered model for the BS to predict the nonlinear time history response.

As shown in Fig. 5, the connection between equipment is established. The order of equipment and their spacing are selected based on a substation data in Tehran. The modal analysis is conducted on the whole connected system. As is obvious from Table 3, the natural frequency of connected system falls between natural frequencies of equipment in the unconnected configuration. The similar phenomena are also observed in Ref. [9]. In the next section, the results of dynamic analysis on stand-alone and interconnected configuration of equipment are presented.

## 4. Analysis

### 4.1. Ground motion input

Far-field ground motion suite of FEMA P695 [36] was chosen as the input to be applied on equipment models given in previous section. Owing to the cantilever nature of insulators, the vertical component of ground motions was also considered in each set [19]. Due to the absence of vertical component of one ground motion set, it was removed from the suite and a total of 21 ground motion sets remained. These records were scaled from 0.1 g to 1.5 g to be appropriate for IDA.

### 4.2. Time history analysis

Nonlinear time history analysis was conducted by employing Newmark time-integration method. Norm displacement increment with  $1.0 \times 10^{-8}$  tolerance and 100 maximum iterations is used as convergence test. It is concluded that these values lead to the convergence for all considered records. Also, based on IEEE 693 recommendation, 2% damping ratio is assumed for each equipment [25].

As reported in previous studies ([1,2,19,27]), the most common failure mode is related to the stresses induced by the bending moment at bottom of equipment where it is connected to the supporting structure. On the other hand, if the relative displacement between

equipment exceeds the displacement capacity of bus slider, the connector loses its flexibility and large forces transfer between the equipment. Thus, the stress at bottom of insulators and the displacement on top where they connect to adjacent equipment are recognized as the key response parameters and are recorded during the analysis.

It is assumed in the analysis process of interconnected equipment that the loss of functionality of each equipment (i.e., reaching 50% of ultimate strength) occurs before the complete collapse of other ones. Therefore, the connection remains between the equipment until the loss of functionality of all of them. This assumption is made due to the uncertainties involved in the estimation of collapse as discussed in section 2.2. Also, unknown impact of collapsed equipment on the adjacent ones was another reason for this assumption.

## 5. Results and discussion

### 5.1. Effect of interaction on responses

To investigate the effect of interaction on the responses, as in Ref. [4], the response ratio is defined as follows

$$R = \frac{\max |u(t)|}{\max |u_0(t)|} \quad (12)$$

where  $u_0(t)$  and  $u(t)$  denote the response of equipment at the unconnected and connected systems, respectively. The response ratio equal to 1 indicates that there is no interaction effect between the equipment, whereas the values larger and smaller than 1 demonstrate the amplification and de-amplification of responses, respectively, due to the presence of intermediate conductor.

Taking surge arrester as an example, Fig. 6 represents the displacement and stress response ratios as a function of PGA for each ground motion set before reaching the displacement limit of bus slider. The truncated results are due to the modeling assumptions described in section 3.6. As seen in Fig. 6, some ground motions cause the amplification of response, while others lead to the suppression. This indicates the complexity of connected system of equipment when more than two equipment are connected together, which is the case for real substations. Moreover, there is a significantly high discrepancy between the response ratios at each intensity level. For instance, at PGA level of 0.1 g, the displacement response ratios range from 0.4 to 1.4. Nevertheless, this discrepancy is slightly reduced with the increase in the intensity. This is because of the difference between the ground motions characteristics, which reveals that extensive analyses are required to accurately determine the response ratio for each equipment. These ratios may be used for the seismic design of new equipment, which

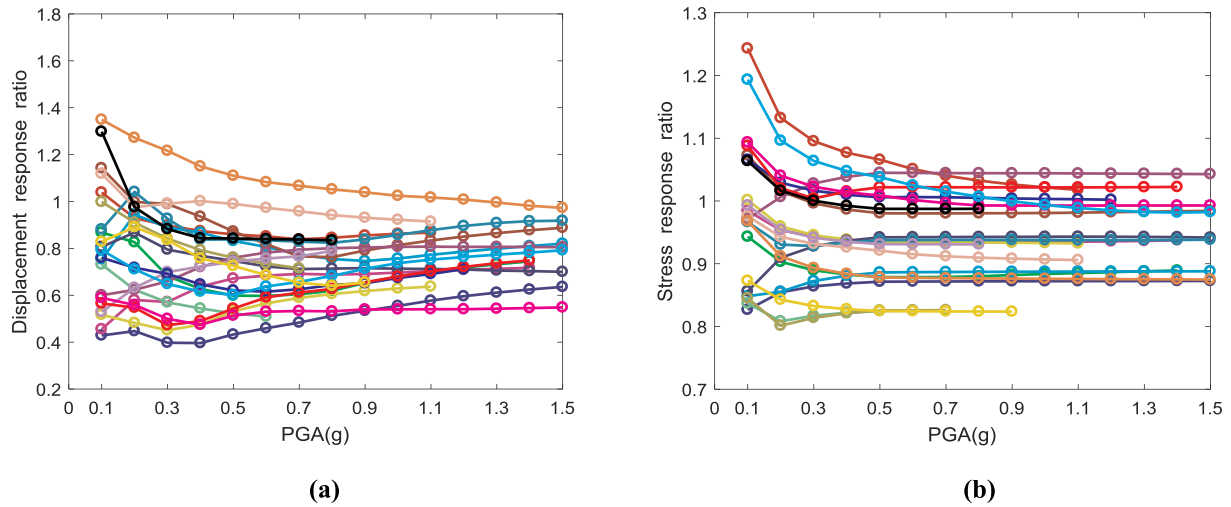


Fig. 6. Response ratios of (a) displacement and (b) stress for surge arrester versus intensity measure.

accounts for the interaction effects without the need to consider adjacent equipment.

As seen in Fig. 6, the variations of response ratios are large at low intensity level for each ground motion, while these variations may be smoother as the intensity level is increased. Furthermore, In the case of ground motions caused amplification, the response ratios approach to 1, when the PGA level is increased. These can be attributed to the high stiffness of rigid bus assembly before the shaft slides at low intensity level and to the increase in the energy dissipation capability of BS as the intensity measure is increased. They are consistent with the conclusion drawn in Ref. [11].

The comparison of Fig. 6a with Fig. 6b indicates that in the case of each individual ground motion, the response ratios are not the same for the displacement and stress responses.

Fig. 7 compares the distribution of response ratios between equipment at PGA level equal to 0.1 g in the box plot. There is a greater variability in CB and DS compared to SA and CT. This can be attributed to the configuration of CB and DS which are more complex than the cantilever-like equipment such as SA or CT. Therefore, the variations of ground motion characteristics such as frequency content have more influence on the interaction results of equipment where the contribution of higher modes is considerable. Similar to SA whose results were mentioned above, absolute amplification or de-amplification is not observed for other equipment. In other words, the maximum ratios of all equipment are larger than 1 and the minimum ratios are smaller than 1. The comparison between Fig. 7a and b reveals that the amplification of stress responses are severe than that of displacement responses for all equipment except for the surge arrester.

For the displacement range allowed by the BS, the results reveal that on average, the energy dissipation capability of BS contributes to the reduction of negative interaction effects. While cable-connected equipment with low level of slack usually creates severe interaction effects and high transfer of force between the equipment as indicated in previous studies ([10,15,16]). Increasing the slack of cables for reducing the interaction effects may violate the clearance requirement of electrical equipment. However, the slider displacement capacity can simply be increased by increasing the shaft length without any influence on the clearance. These results show some advantages of BS over cables as conductor.

5.2. Equipment fragility

In order to show the procedure described in section 2.2 for generating the fragility curves, the maximum stresses at bottom of DS

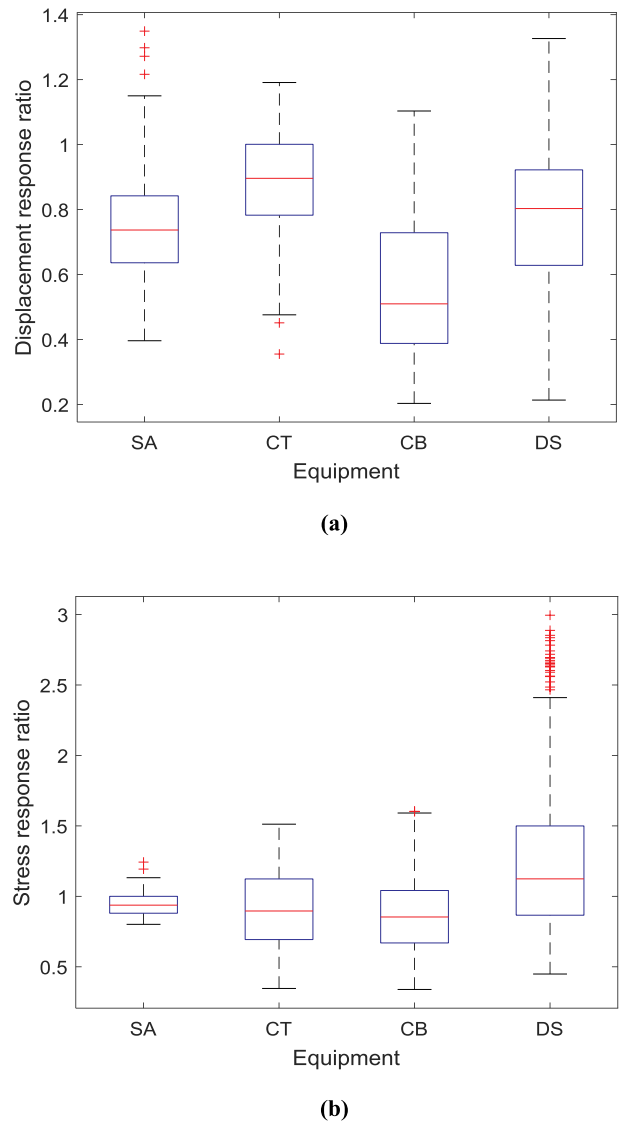


Fig. 7. Box plots of (a) displacement and (b) stress response ratios for each equipment at PGA = 0.1 g.

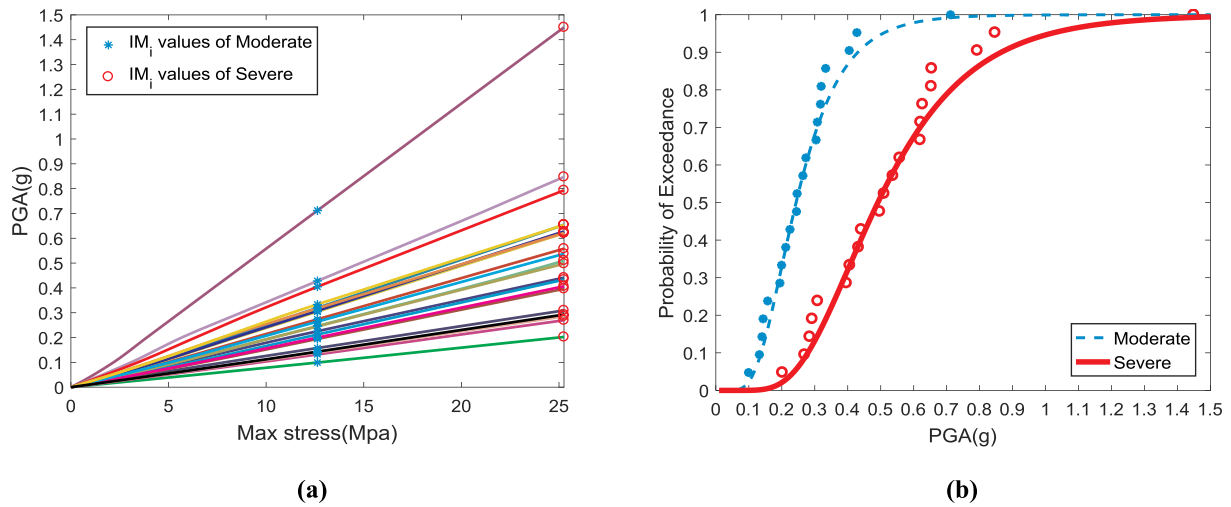


Fig. 8. (a) Maximum stress at bottom of DS post insulators versus PGA (b) fitted fragility function along with cumulative distribution data.

insulators as a function of PGA are depicted in Fig. 8a for the suite of ground motions. Also, the  $IM_i$  values are demonstrated in this figure where each ground motion exceeds the damage state threshold. To determine the cumulative probability of exceedance at each  $IM_i$ , the number of records causing exceedance at lower intensity levels is divided by the total number of records. Fig. 8b shows the obtained values along with the fitted lognormal distribution by Equations (2) and (3). The relatively close agreement depicts the suitability of selected method for the fitting. Furthermore, as can be seen in Fig. 8a, the relatively small dispersion of maximum stress given PGA implies the suitability of PGA as an intensity measure for IDA analysis [37]. This is also the case for other equipment where the stress responses are not shown here for the sake of brevity.

Figs. 9–12 illustrate the fragility curves generated for the surge arrester, current transformer, circuit breaker, and disconnect switch in the connected and unconnected configurations. Considering the conductors leads to the increase in the vulnerability of DS; however, for other three equipment, accounting for the connection between the equipment results in the reduction of vulnerability. The reduction in the vulnerability of three out of four equipment in the connected condition may be related to the high damping capacity of bus slider. Another reason is perhaps the movement restriction induced by the conductors especially at out-of-plane direction of conductors.

The fragility parameters for the equipment in the stand-alone and

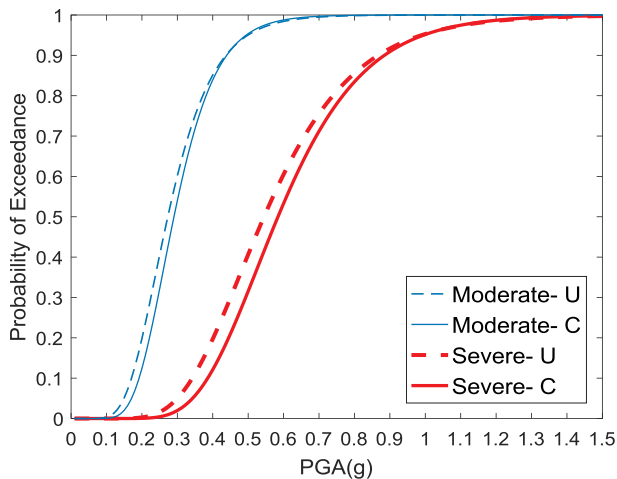


Fig. 9. Fragility curves of surge arrester in unconnected (U) and connected (C) systems.

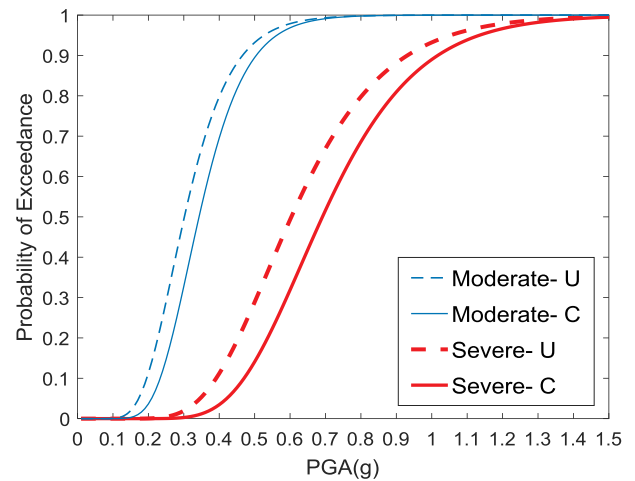


Fig. 10. Fragility curves of current transformer in unconnected (U) and connected (C) systems.

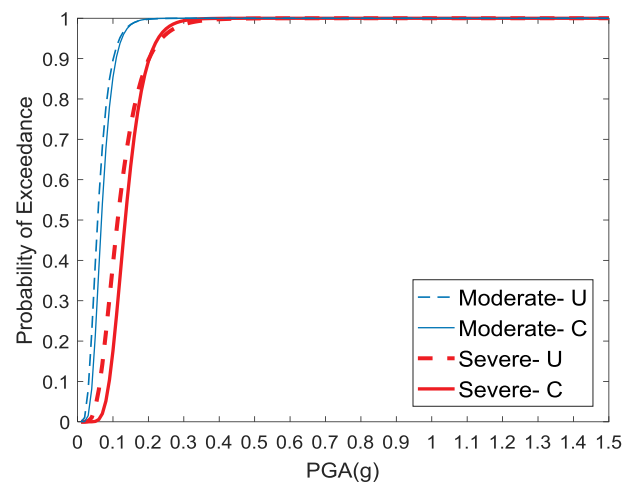


Fig. 11. Fragility curves of circuit breaker in unconnected (U) and connected (C) systems.

interconnected system are listed in Table 7 and Table 8, respectively. The comparison of median values reveals that accounting for the interaction has the most influence on the CB reduction by about 19% and DS increase by about 13%. The CB in stand-alone configuration and the

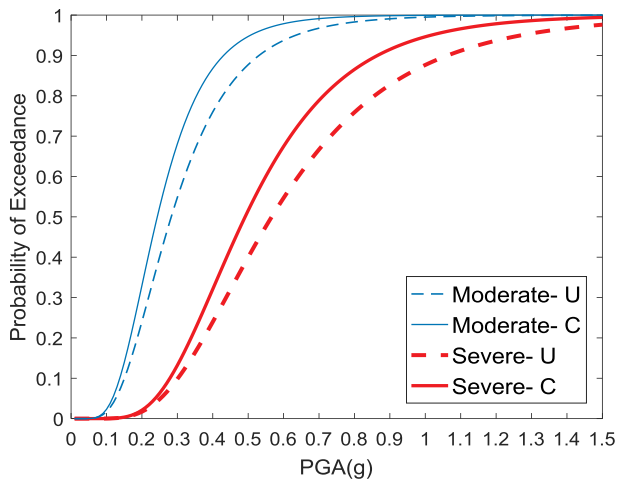


Fig. 12. Fragility curves of disconnect switch in unconnected (U) and connected (C) systems.

Table 7

Fragility curve parameters for equipment in stand-alone configuration (unconnected):  $\theta$ : median (in g) and  $\beta$ : standard deviation.

Equipment	Moderate		Severe	
	$\theta$	$\beta$	$\theta$	$\beta$
Surge arrester	0.27	0.37	0.54	0.36
Current transformer	0.30	0.34	0.60	0.34
Circuit breaker	0.06	0.45	0.11	0.45
Disconnect switch	0.28	0.49	0.57	0.49

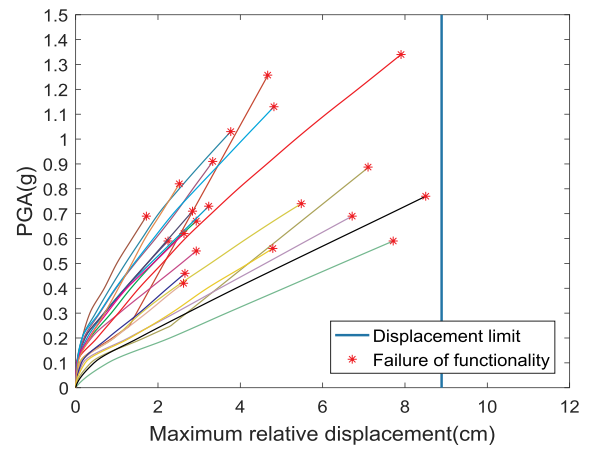
Table 8

Fragility curve parameters for equipment in bus slider-connected system (connected):  $\theta$ : median (in g) and  $\beta$ : standard deviation.

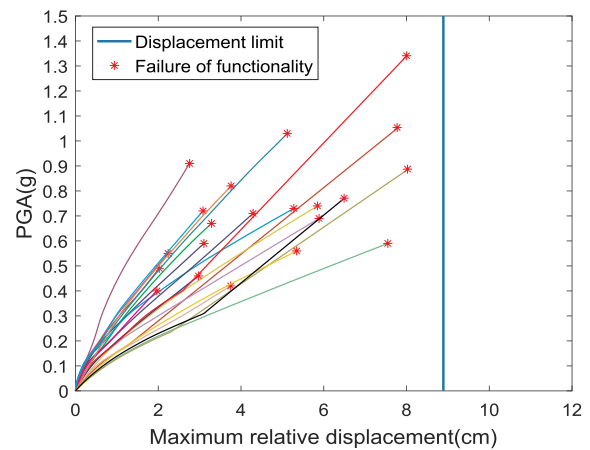
Equipment	Moderate		Severe	
	$\theta$	$\beta$	$\theta$	$\beta$
Surge arrester	0.29	0.32	0.58	0.32
Current transformer	0.34	0.30	0.69	0.30
Circuit breaker	0.07	0.37	0.13	0.32
Disconnect switch	0.24	0.44	0.49	0.44

CT in interconnected system depict the highest and smallest fragility, respectively. SA has more vulnerability than DS in the stand-alone configuration, while this order is reverse in the interconnected system. The median value of PGA for SA is about 4% smaller than that for DS in the unconnected configuration. However, the median value of PGA for DS is 19% smaller than that for SA in the connected configuration. These results indicate that considering the interaction between the equipment may alter the vulnerability order of equipment, which is important for the utility managers who want to decide on the prioritization of equipment for retrofiting. Comparing dispersion parameters ( $\beta$ ) shows the decrease in the case of connected equipment relative to the unconnected ones.

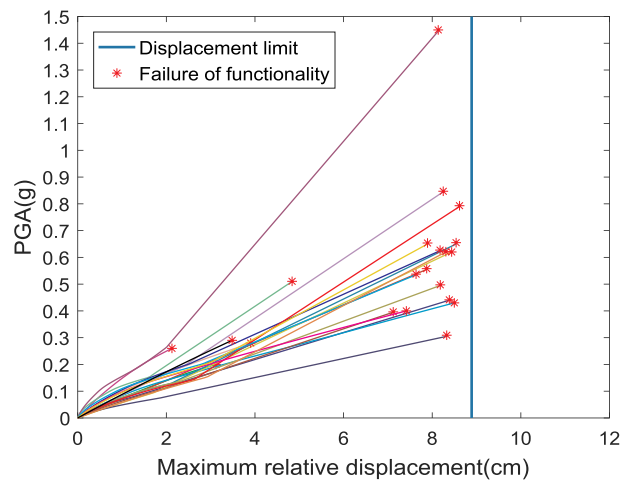
As mentioned in section 3.6, the assumption made for the modeling of interconnected equipment neglects the impact caused by the violation of BS displacement limit. In order to examine the effect of this assumption on the fragility results, the maximum relative displacement between two adjacent equipment is plotted against PGA in Fig. 13. In case of each record, this curve is continued up to PGA level where the loss of functionality occurs for the both adjacent equipment. Obviously, the failure of functionality occurs before reaching the displacement limit of BS. Thus, this assumption has no effect on the fragility functions developed here. It is also worth noting that if the displacement of



(a)



(b)



(c)

Fig. 13. IDA analysis results of relative displacement between (a) LA and CT (b) CT and CB (c) CB and DS.

conductors goes beyond capacity during the seismic excitation, the interaction effects may be more intensive than what is observed in the present study. The non-occurrence of this phenomena before the failure of functionality can be attributed to the relatively low difference between the frequencies of interconnected equipment.

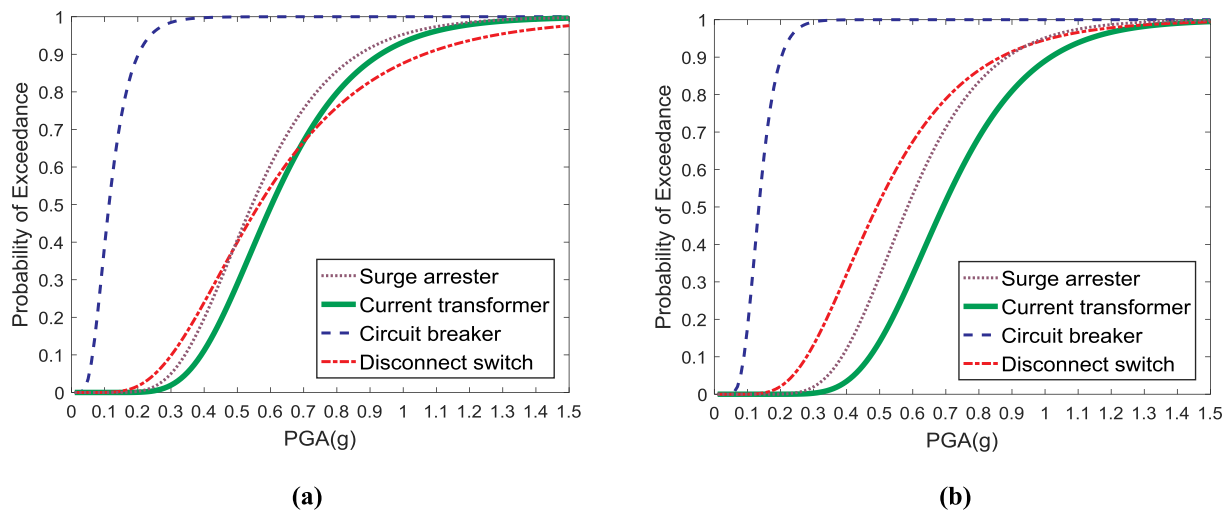


Fig. 14. Comparison of fragility curves of severe damage states for equipment items in stand-alone configuration (a), and in bus slider-connected system (b) with each other.

According to equipment catalog, the ultimate resisting force of terminal pad that connects the BS to the equipment is about 3000 N. As is obvious from BS cyclic curves in Fig. 3b, the induced forces in BS when reaching to the displacement limit (i.e., 8.89 cm) are lower than 1500 N. Therefore, it can be deduced from Fig. 13 that severe damage state occurred before the pad failure.

Fig. 14 compares the vulnerability of equipment with each other at the connected and unconnected systems. CB was the most fragile equipment in both cases. The large difference between the vulnerabilities of this equipment in comparison with others can be attributed to the large concentrated mass with the eccentricity relative to main insulator column, which is not the case for other equipment. This result could not be obtained if SDOF system was used to model the equipment. For the unconnected case, DS was the second most vulnerable equipment at lower intensity level, which was replaced with SA at PGA levels higher than 0.5 g. This replacement occurs at higher PGA (0.9 g) for the connected case. CT is the least fragile equipment in the connected case, whereas it is replaced with DS at the intensity levels higher than 0.7 g in the unconnected case.

5.3. Comparison with other studies

In order to investigate the difference between the fragility curves

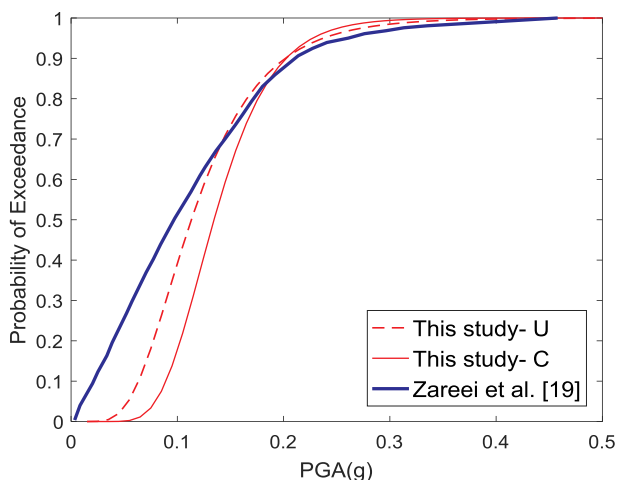


Fig. 15. Comparison of generated fragility curves for severe damage state of circuit breaker with Zareei et al. [19].

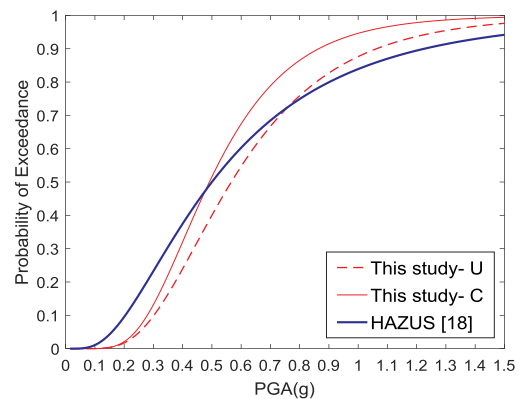


Fig. 16. Comparison of generated fragility curves for severe damage state of disconnect switch with HAZUS [18].

presented here and those proposed in previous studies, the fragility curves of circuit breaker and disconnect switch are compared with those of Zareei et al. [19] and HAZUS [18] in Fig. 15 and Fig. 16, respectively. In the first study, the analytical fragility curve of circuit breaker is proposed according to its stand-alone configuration. As can be seen in Fig. 15, the fragility results proposed here for the stand-alone circuit breaker have more agreement than the bus slider-connected circuit breaker, particularly at high intensity levels. Note that this separation can be justified by the difference between the configurations of two equipment. On the other hand, the fragility curves proposed by HAZUS for the equipment are based on the observation of damages at substations in previous earthquakes and thus, the conductors between the equipment may influence on their vulnerability. Also, due to the high diversity of equipment and conductors of the considered substations, the proposed vulnerability functions are probably a rough estimate of actual ones. As is obvious from Fig. 16, the median of bus slider-connected disconnect switch is almost equal to the one proposed by HAZUS. However, owing to the high dispersion of HAZUS functions, this agreement is not made at other intensity levels. This high dispersion can be attributed to the real uncertainty considered in HAZUS.

5.4. Accuracy of fragility curves

As described in section 2.3, the Monte Carlo approach was utilized to examine the efficiency of fragility parameters. A set of 10,000 simulations was conducted each one including a set of 21 numbers of

**Table 9**  
Standard error of considered accuracy metrics for stand-alone equipment items.

	SA		CT		CB		DS	
	DS1 <sup>a</sup>	DS2 <sup>b</sup>	DS1	DS2	DS1	DS2	DS1	DS2
COV of $\theta$ (%)	7.99	7.91	7.30	7.30	9.83	9.89	10.73	10.82
COV of $\beta$ (%)	15.88	16.04	15.88	16.06	12.21	15.55	15.96	16.36
COV of $\lambda_{failure}$ (%)	–	18.51	–	17.59	–	23.63	–	27.47
Bias $\theta$ (%)	0.42	0.43	0.32	0.33	0.85	0.60	0.44	0.54

<sup>a</sup> DS1 is corresponding to moderate damage state.

<sup>b</sup> DS2 is corresponding to severe damage state.

synthetic structural analysis data. Thus, 10,000 estimations of fragility parameters (i.e.,  $\theta$  and  $\beta$ ) were at hand, which are used to calculate the efficiency metrics. Two metrics considered similar to Ref. [23] are:

- 1) Coefficient of variation (COV) of simulated fragility parameters and annual rate of failure for a given hazard curve.
- 2) Difference between mean of simulated parameters for  $\theta$  (i.e., median of fragility curve) and original one.

When the bound of parameter estimations (i.e., standard deviation) is narrower, the accuracy of estimation is higher. The higher level of accuracy means that the parameter estimation is more stable, in spite of the record-to-record uncertainty involved in the analysis. On the other hand, if the mean of estimated parameters from the simulation differs from the true ones, the model is biased, indicating that the estimated fragility parameters are unstable. This can be decreased by increasing the number of ground motion in IDA [23].

Table 9 and Table 10 summarize the computed metrics of two damage states for the equipment in the stand-alone and connected systems. The calculation of  $\lambda_{failure}$  is based on the procedure described in section 2.4 and the hazard curve shown in Fig. 18. The COV of medians is lower than 10%, and the bias of this parameters is less than 1% for all considered cases. These ranges are recommended by Ref. [23]. Thus, all the developed fragilities have acceptable level of accuracy. Taking into account the first metric reveals that the fragility function of CT in the connected system including the lowest COVs has the most accuracy, while the DS function has the least accuracy. This is probably because of the higher dispersion of responses for DS in comparison with other ones.

### 5.5. Various interconnected systems

As is known, in all substations, several equipment is connected to each other. To explore how many interconnected equipment can have a substantial impact on the vulnerability of equipment, different connected systems are considered for each equipment item, and the fragility functions are generated for each system. Fig. 17a–d shows these functions for various systems of each equipment. The legend of the figures denotes what equipment is connected together. Also, the modal frequencies of connected systems are reported in Table 11. Although the studied systems are limited, some observations discussed below can

**Table 10**  
Standard error of considered accuracy metrics for interconnected equipment items.

	SA		CT		CB		DS	
	DS1	DS2	DS1	DS2	DS1	DS2	DS1	DS2
COV of $\theta$ (%)	7.00	7.03	6.52	6.53	8.08	6.89	9.65	9.59
COV of $\beta$ (%)	15.91	16.11	15.82	16.04	7.94	11.00	16.01	16.19
COV of $\lambda_{failure}$ (%)	–	18.51	–	17.59	–	23.63	–	27.47
Bias $\theta$ (%)	0.28	0.28	0.22	0.24	0.86	0.41	0.54	0.56

be made.

Fig. 17a and b demonstrate that when DS or CB is connected to the systems, the vulnerability of equipment is considerably changed. This can be attributed to the contribution of other modes rather than first mode to the responses of these equipment due to their configuration.

For the equipment similar to SA and DS (Fig. 17a and d), which are placed at the end of the systems and other equipment is connected only from one side, only the nearest equipment has a substantial effect. Therefore, the connection to other equipment can be neglected in the analysis. In the case of SA, all types of connected systems cause to decrease in the vulnerability. However, considering all kinds of systems in conjunction with DS leads to the increased fragility.

In case of the equipment like CB and CT, which are connected to other equipment from both sides, considering the connection only through one side may overestimate or underestimate fragility function. For example, in case of CT, taking into account the connection only with SA leads to the slight increase in its vulnerability, while considering the interaction only with CB results in the decrease in its vulnerability (Fig. 17b). Similarly, in case of CB, the connection with CT causes higher fragility at high intensity levels, whereas the interaction with DS leads to the reduction of fragility (Fig. 17c). Thus, it may be nonconservative to consider only two connected equipment. This is in a good agreement with the results in Ref. [16] which investigated the cable-connected equipment. For the equipment located in the middle of systems, it is recommended to consider the connection to both adjacent equipment.

The indirectly connected equipment can be neglected in the analysis if the contribution of higher modes to their response is small. These results are more important when they are intended for the loss estimation of entire substation, and it may not be computationally feasible to consider all of the equipment connected to each other.

## 6. Failure probability evaluation

In previous sections, the comparison between the vulnerabilities of equipment was dependent on the intensity measure. In order to have an overall view, the failure fragility curves are coupled with the seismic hazard curve throughout the range of intensity measures, which yields an estimation of failure probability independent of  $IM$ . Therefore, the effect of each intensity level according to their weight in the hazard curve is incorporated in the fragility results. For example, the seismic hazard curve of a site in Tehran, which is produced in Ref. [38], is presented in Fig. 18 and Equations (4) and (5) are employed to compute the probability of failure of equipment in 50 years. Table 12 presents the failure probabilities for each equipment in the stand-alone and four-connected-equipment configurations. Although the order of vulnerable equipment is not changed for this particular hazard curve owing to the presence of conductors, the probability of failure of CT and DS is reduced by 30% and increased by 22%, respectively, which confirms the importance of considering the conductor between the equipment.

## 7. Conclusions

This paper investigates the seismic response of various connected equipment relative to the stand-alone ones when more than two equipment is connected to each other. Three dimensional models are used to represent the equipment. The fragility functions are produced for the equipment in both connected and unconnected configurations. Based on this study, the following conclusions can be drawn:

- The response ratios of equipment in connected systems to unconnected ones are highly dependent on the ground motion characteristics. For example, the displacement response of SA shows the amplification by 40% when subjected to Chi-Chi (1999, Taiwan) record. However, the suppression of response by 60% is observed when subjected to Northridge (1994, US) ground motion.

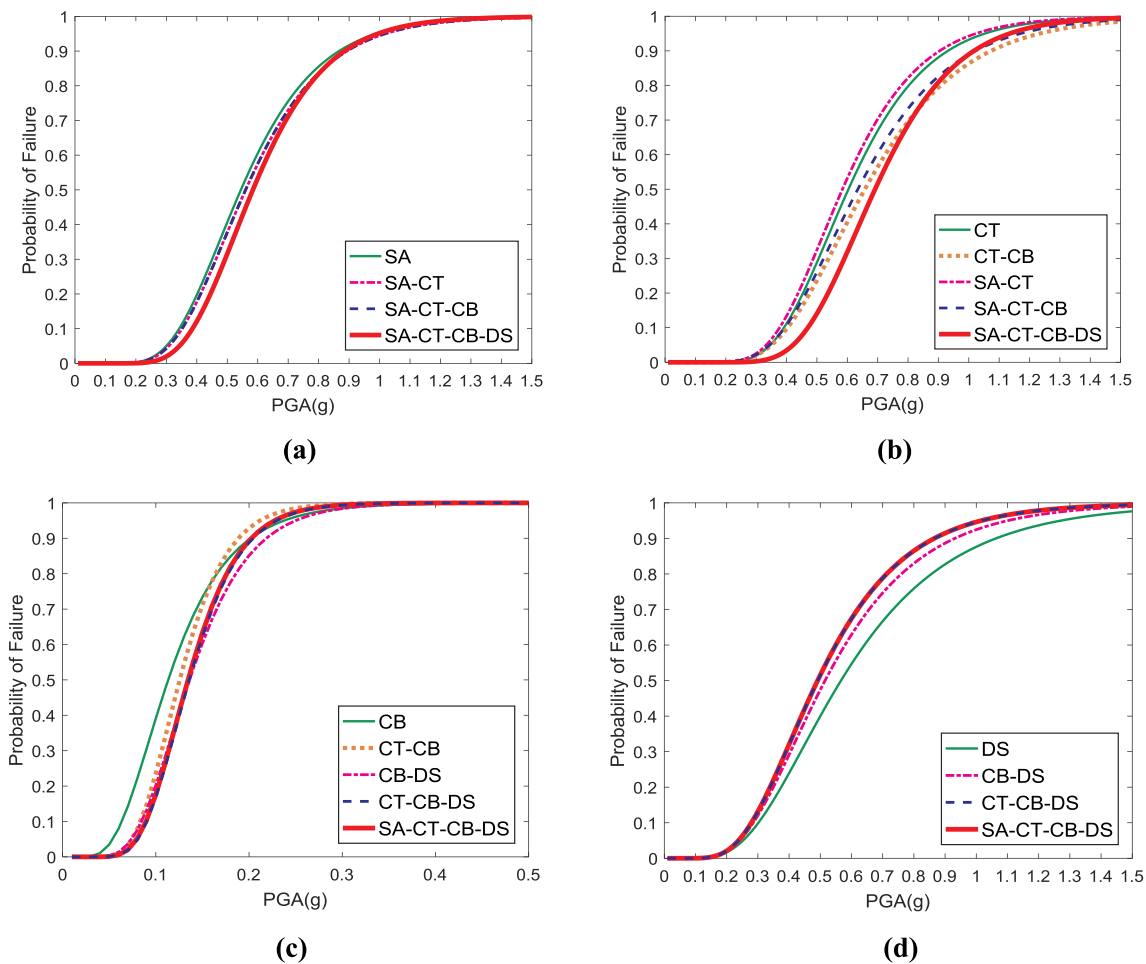


Fig. 17. Fragility curves of severe damage state for (a) surge arrester, (b) current transformer, (c) circuit breaker, and (d) disconnect switch in different connected systems.

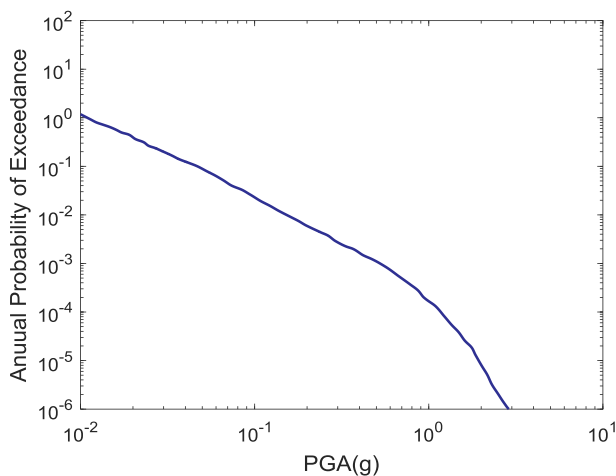


Fig. 18. Hazard curve of a typical site in Tehran [38].

- The variations of ground motion characteristics such as frequency content result in further variation in the response ratio of equipment, whose contribution of higher modes to the responses are notable.
- For the displacement range allowed by the BS, on average, considering the connection between the equipment reduced both the displacement and the stress responses due to the high energy dissipation capability of bus slider. However, this pattern may be

Table 11

Frequency results of connected systems.

item	Mode 1	Mode 2	Mode 3	Mode 4	Mode 5
SA-CT	3.64	3.79	4.4	10.88	19.7
CT-CB	2.55	3.16	3.66	4.9	6.22
CB-DS	1.75	2.3	2.52	2.96	5.89
SA-CT-CB	2.55	3.26	3.66	4.39	4.91
CT-CB-DS	1.77	2.62	2.88	3.33	3.94
SA-CT-CB-DS	1.77	2.62	2.96	3.33	3.93

Table 12

Probability of failure in 50 years for unconnected (U) and connected (C) equipment systems.

Equipment item	Probability of failure in 50 years (%)
SA-U	5.44
SA-C	4.48
CT-U	4.24
CT-C	2.97
CB-U	77.63
CB-C	57.48
DS-U	6.16
DS-C	7.50

changed if the bus slider goes beyond its capacity during the excitation.

- In the case when ground motions cause the amplification of responses in the connected systems, the increase in the intensity level

results in the reduction of interaction effect. This can be attributed to the high energy dissipation capability of bus slider at large intensity levels.

- The interaction between equipment has a significant effect on their fragility. For instance, it leads to the increase in probability of failure of DS by 22% and the decrease of CT by 30% for a substation site in Tehran. Therefore, the reliable seismic risk evaluation of substations requires the consideration of conductor effects.
- The effect of interaction on fragility may vary depending on the dynamic characteristics of the equipment and those to which are connected, even those that are indirectly connected.
- In spite of almost equal large concentrated mass on top of both CB and CT, the significant difference between their vulnerabilities may be attributed to the eccentricity of CB lumped mass relative to its main insulator, which increases the contribution of torsional modes. This result cannot be observed by modeling the equipment as SDOF systems, and it reveals the importance of 3D modeling of equipment.
- In the unconnected conditions, the median parameter of fragility function for SA was about 4% smaller than that for DS, while in the connected conditions, the median parameter of fragility function for DS was 19% smaller than that for SA. This change in the order of more vulnerable equipment reveals the significance of considering the interaction for the retrofit prioritization.
- Comparing the vulnerability of individual equipment in various three- and four-connected equipment systems demonstrated that accounting for non-adjacent equipment in vulnerability assessment is required when the contribution of higher modes to its response is significant.

## References

- [1] Alessandri S, Giannini R, Paolacci F, Malena M. Seismic retrofitting of an HV circuit breaker using base isolation with wire ropes. Part 1: preliminary tests and analyses. *Eng Struct* 2015;98:251–62. <https://doi.org/10.1016/j.engstruct.2015.03.032>.
- [2] Li S, Tsang HH, Cheng Y, Lu Z. Considering seismic interaction effects in designing steel supporting structure for surge arrester. *J Constr Steel Res* 2017;132:151–63. <https://doi.org/10.1016/j.jcsr.2017.01.012>.
- [3] Paolacci F, Giannini R, Alessandri S, De Felice G. Seismic vulnerability assessment of a high voltage disconnect switch. *Soil Dynam Earthq Eng* 2014;67:198–207. <https://doi.org/10.1016/j.soildyn.2014.09.014>.
- [4] Der Kiureghian A, Sackman JL, Hong KJ. Interaction in interconnected electrical substation equipment subjected to earthquake ground motions. PEER; 1999.
- [5] Gilani AS, Whittaker AS, Fenves GL, Chen CH, Ho HFE. Seismic evaluation and analysis of 230-kV disconnect switches. PEER; 2000.
- [6] Takhirov SM, Fenves GL, Fujisaki E. Seismic qualification and fragility testing of line break 550-kV disconnect switches. PEER; 2005.
- [7] Kong D. Evaluation and protection of high voltage electrical equipment against severe shock and vibrations Phd Diss Dep Civil Struct Environ Eng State Univ New York Buffalo; 2010.
- [8] Mosalam KM, Günay STS. Response evaluation of interconnected electrical substation equipment using real-time hybrid simulation on multiple shaking tables. *Earthq Eng Struct Dyn* 2016;45:2389–404. <https://doi.org/10.1002/eqe>.
- [9] Filiatrault AKS. Seismic interaction of interconnected electrical substation equipment. *J Struct Eng* 2000;126:1140–9. [https://doi.org/10.1016/S0950-1401\(10\)04009-7](https://doi.org/10.1016/S0950-1401(10)04009-7).
- [10] Der Kiureghian A, Hong K-J, Sackman JL. Further studies on seismic interaction in interconnected electrical substation equipment. PEER; 2000.
- [11] Stearns C, Filiatrault A. Electrical substation equipment Interaction : experimental rigid conductor studies. PEER; 2004.
- [12] Song J, Der Kiureghian KSJ. Seismic response and reliability of electrical substation equipment and systems. Berkeley: Doctoral Diss Univ California; 2004. <https://doi.org/10.1017/CBO9781107415324.004>.
- [13] Dastous JBDKA. Application guide for the design of flexible and rigid bus connections between substation equipment subjected to earthquakes. PEER; 2010.
- [14] Dastous J-B, Pierre J-R. Design methodology for flexible buswork between substation equipment subjected to earthquakes. *IEEE Trans Power Deliv* 2007;22:1490–7.
- [15] Mohammadi RK, Nikfar F, Akrami V. Estimation of required slack for conductors connecting substation equipment subjected to earthquake. *IEEE Trans Power Deliv* 2012;27:709–17.
- [16] Mohammadi RK, Tehrani AP. An investigation on seismic behavior of three interconnected pieces of substation equipment. *IEEE Trans Power Deliv* 2014;29:1613–20.
- [17] Anagnos T. Development of an electrical substation equipment performance database for evaluation of equipment fragilities. PEER; 1999. <https://doi.org/10.2307/3831246>.
- [18] Mr HM. Multi-hazard loss estimation methodology: earthquake model. Washington, DC: Dep Homel Secur FEMA; 2003.
- [19] Zareei SA, Hosseini M, Ghafory-Ashtiani M. Evaluation of power substation equipment seismic vulnerability by multivariate fragility analysis: a case study on a 420 kV circuit breaker. *Soil Dynam Earthq Eng* 2017;92:79–94. <https://doi.org/10.1016/j.soildyn.2016.09.026>.
- [20] Kitayama S, Constantinou M, Lee D. Procedures and results of assessment of seismic performance of seismically isolated electrical transformers with due consideration for vertical isolation and vertical ground motion effects. Tech Rep MCEER-16-0010. Buffalo, NY: Multidiscip Cent Earthq Eng Res Univ Buffalo; 2016.
- [21] Zareei SA, Ghafory-Ashtiani M. Seismic failure probability of a 400 kV power transformer using analytical fragility curves. *Eng Fail Anal* 2016;70:273–89. <https://doi.org/10.1016/j.engfailanal.2016.09.007>.
- [22] Vamvatsikos D, Cornell CA. Incremental dynamic analysis. *Earthq Eng Struct Dyn* 2002;31:491–514. <https://doi.org/10.1002/eqe.141>.
- [23] Baker JW. Efficient analytical fragility function fitting using dynamic structural analysis. *Earthq Spectra* 2015;31:579–99. <https://doi.org/10.1193/021113EQS025M>.
- [24] Ibarra LFKH. Global collapse of frame structures under seismic excitations. Stanford: John A Blume Earthq Eng Center; 2005. <https://doi.org/10.1002/eqe>.
- [25] IEEE Standard 693. IEEE recommended practice for seismic design of substations. (Revision of IEEE 693-1985 & 1997). 2005.
- [26] ASCE-7. Minimum design loads and associated criteria for buildings and other structures. 2017. <https://doi.org/10.1061/9780784414248>.
- [27] Mohammadpour S, Hosseini M. Experimental system identification of a 63kV substation post insulator and developing its fragility curves by dynamic finite element analyses. *Earthq Spectra* 2017;33:1149–72.
- [28] Moustafa MA, Mosalam KM. Structural performance of porcelain and polymer post insulators in high voltage electrical switches. *J Perform Constr Facil* 2016;30. [https://doi.org/10.1061/\(ASCE\)CF.1943-5509.0000848](https://doi.org/10.1061/(ASCE)CF.1943-5509.0000848).
- [29] Medina RA, Krawinkler H, Alavi B. Seismic demand for nondeteriorating frame structures and their dependence on ground motion. *Eng Struct* 2003;25:637–53. [https://doi.org/10.1016/S0141-0296\(02\)00174-8](https://doi.org/10.1016/S0141-0296(02)00174-8).
- [30] Eads L, Miranda E, Krawinkler HLD. An efficient method for estimating the collapse risk of structures in seismic regions. *Earthq Eng Struct Dyn* 2013;42:25–41. <https://doi.org/10.1002/eqe>.
- [31] Alessandri S, Giannini R, Paolacci F, Amoretti M, Freddo A. Seismic retrofitting of an HV circuit breaker using base isolation with wire ropes . Part 2 : shaking-table test validation. *Eng Struct* 2015;98:263–74. <https://doi.org/10.1016/j.engstruct.2015.03.031>.
- [32] McKenna F, Fenves G, Filippou FCMS. Open system for earthquake engineering simulation. 2000. OpenSees.
- [33] Li S, Tsang HH, Cheng ZCL YF. Effects of sheds and cemented joints on seismic modelling of cylindrical porcelain electrical equipment in substations. *Earthquakes Struct* 2017;12:55–65.
- [34] Hakimi BE, A SA. Design of energy dissipator devices to protect equipments of a 400 kv power substation against earthquake in Neishbour-Iran. 13 th World Conf. Earthq. Eng 2004:3262.
- [35] Whittaker AS, Fenves GL, Gilani ASJ. Seismic evaluation and analysis of high-voltage substation disconnect switches. *Eng Struct* 2007;29:3538–49. <https://doi.org/10.1016/j.engstruct.2007.07.028>.
- [36] P695 FEMA. Quantification of building seismic performance factors. Washington, DC: Fed Emerg Manag Agency; 2009. <https://doi.org/10.1016/j.compstruc.2009.08.001>.
- [37] Vamvatsikos D, Cornell CA. Applied incremental dynamic analysis. *Earthq Spectra* 2004;20:523–53. <https://doi.org/10.1193/1.1737737>.
- [38] Gholipour Y, Bozorgnia Y, Rahnama M, Berberian MSJ. Probabilistic seismic hazard analysis, phase I-greater Tehran regions. Final Report 2008;1.